Negative-parity structures and lifetime measurements in ^{71}As

R.S. Zighelboim, S.G. Buccino, and F.E. Durham
Department of Physics, Tulane University, New Orleans, Louisiana 70118

J. Döring, P.D. Cottle, J.W. Holcomb,* T.D. Johnson,† S.L. Tabor, and P.C. Womble‡
Department of Physics, Florida State University, Tallahassee, Florida 32306
(Received 23 March 1994)

High-spin states up to $(\frac{29}{2}^+)$ and $(\frac{29}{2}^-)$ in ^{71}As have been studied via the ^{58}Ni(^{19}F,$\alpha 2p$) reaction at 62 MeV using in-beam γ-ray spectroscopic techniques. Based on a particle-γ coincidence measurement a new decay sequence of negative parity has been assigned to ^{71}As. Lifetimes for some $E2$ transitions were extracted from Doppler-shifted line shapes observed in coincidence mode, and experimental transition quadrupole moments were determined. They indicate a moderate to high collectivity in both the positive-parity yrast band and the new negative-parity decay sequence at high spins. Total Routhian surfaces calculated for states of both parities reveal strong triaxial shapes at high spins. A noncollective structure of $\frac{19}{2}^{(-)}$ and $\frac{21}{2}^{(-)}$ states is interpreted as a three-quasiparticle excitation.

PACS number(s): 21.10.Tg, 23.20.Lv, 27.50.+e

I. INTRODUCTION

The odd-mass As isotopes provide an excellent series to study the shape coexistence effects that occur in the transitional light isotopes of the *fpg* subshells. Much is known about the high-spin structure of the neighboring even-even Ge and Se nuclei in this mass region, but less is understood about the odd-mass nuclei. In the odd-mass As isotopes the first $\frac{9}{2}^+$ level occurs at excitation energies ranging downward from 1422 keV in ^{67}As [1] to 303 keV in ^{75}As [2] and to 475 keV in ^{77}As [3]. Although for $Z = 33$ and neutron numbers near midshell a low-lying $\frac{9}{2}^+$ state arising from the $[404]\frac{9}{2}^+$ Nilsson orbital would imply oblate deformation, particle-plus-rotor calculations suggest strong mixing of the $g_{9/2}$ substates leading to a triaxial shape for ^{71,73}As [4]. The need for more experimental evidence concerning the shape evolution at high spins provides one impetus for further study of these nuclei.

In the present study we have examined the high-spin states of ^{71}As. This isotope, with $N = 38$, lies in the middle of the sequence of As isotopes accessible to high-spin studies through fusion-evaporation reactions. Previous work on ^{71}As provided some information about the spin and parity of the ground state and low-lying states via the Ge(^{3}He,d) transfer reaction [5,6] and via the β decay of ^{71}Se [7], whereas the 1000.2 keV $\frac{9}{2}^+$ isomer in ^{71}As and the positive-parity yrast sequence on top of it were investigated up to spin $\frac{21}{2}\hbar$ via the ^{69}Ga($\alpha, 2n$) and heavy-ion-induced reactions [8–10]. In the latter studies also the lifetimes of some positive-parity states were measured leading to a quadrupole deformation of $\beta_2 \approx 0.29$.

Our interest in studying ^{71}As was to extend the positive-parity band to higher spins, to measure additional transition probabilities, and to search for negative-parity high-spin states which were not known before the present work.

II. EXPERIMENTAL TECHNIQUES

A. Prompt γ-γ coincidence measurement

High-spin states in ^{71}As were studied using the reaction ^{58}Ni(^{19}F,$\alpha 2p$) at a beam energy of 62 MeV. The ^{19}F beam was provided by the Florida State University Tandem accelerator facility. The target consisted of a self-supporting 19 mg/cm^2 foil enriched to 99.9% in ^{58}Ni. Four Ge γ-ray detectors of 25% relative efficiency and a resolution of 2.1 keV at 1.33 MeV were used, three of them Compton suppressed. Two of the Compton-suppressed detectors were positioned at 90° to the beam direction and the third at 4°. The fourth Ge detector was positioned at 140°. The front of each detector was approximately 10 cm away from the target. More than 6 $\times$ 10^8 γ-γ coincidence events were collected on magnetic tape for later analysis. Internal energy calibrations were performed for each detector using a least-squares fit to the energies of the following lines: 74.97 keV (Pb x ray), 188.4 keV (^{74}Br), 197.15 keV (^{19}F), 511.0 keV (e^+e^-), 634.8 keV (^{74}Se), and 1000.2 keV (^{71}As). The coincident γ-γ events were sorted into four two-dimensional matrices corresponding to the four pairs of detector angles. These matrices were analyzed by setting gates on the peaks of

*Present address: Martin Marietta Information Systems, Mail Stop 800, Orlando, FL 32825.
†Present address: II. Physikalisches Institut, Universität Göttingen, D-37073 Göttingen, Federal Republic of Germany.
‡Present address: Oak Ridge National Laboratory, Mail Stop 6388, Oak Ridge, TN 37830.

interest with proper background subtraction. Two examples of gated γ-ray spectra obtained from the (90°-90°) matrix are given in Figs. 1 and 2. A third example as shown in Fig. 3 is taken from the statistically better (90°-4°) matrix.

The (90°-4°) matrix was used to extract relative intensities of γ rays to determine directional correlations of oriented (DCO) nuclei ratios $R_{\rm DCO}$. These values provided information about spin differences for many γ rays and helped to assist in the assignment of level spins. The experimental $R_{\rm DCO}$ ratio is defined in the present work as

$$R_{\rm DCO} = \frac{I(\gamma_1 \text{ observed at } 4^\circ \text{ gated by } \gamma_2 \text{ at } 90^\circ)}{I(\gamma_1 \text{ observed at } 90^\circ \text{ gated by } \gamma_2 \text{ at } 4^\circ)}. \quad (1)$$

The coincidence gating transitions used for the $R_{\rm DCO}$ determinations were always stretched $E2$ transitions. In this case the value for $R_{\rm DCO}$ is expected to be approximately unity for a coincident stretched $E2$ transition, while for a mixed dipole-quadrupole transition the ratio can vary from 0 to 2. However, values near one-half are typical of pure or less mixed dipole transitions between states with a spin difference $\Delta I = 1$. In most cases the results from several gates were compared to determine an average value and uncertainty, and they are listed in Table I. Some details for the different structures in ^{71}As will be discussed in the relevant sections.

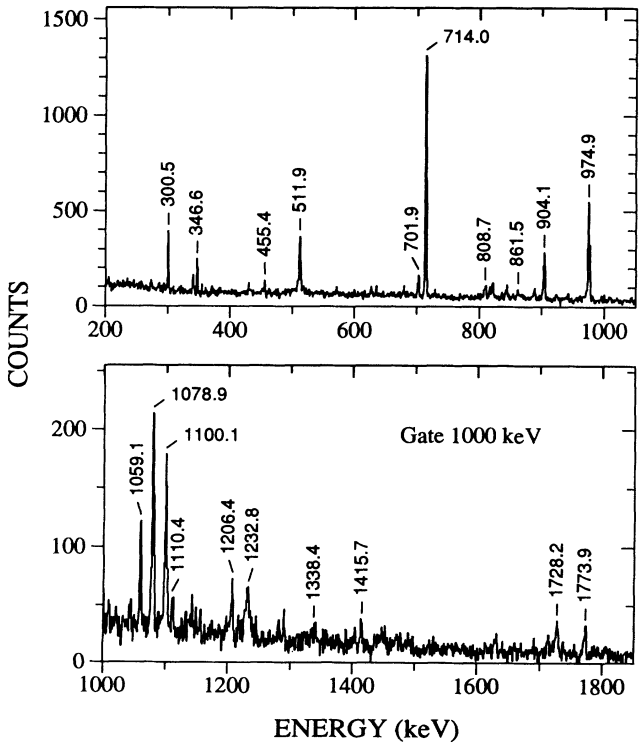

FIG. 1. Background-corrected coincidence spectrum gated on the 1000.2 keV transition in the (90°-90°) matrix.

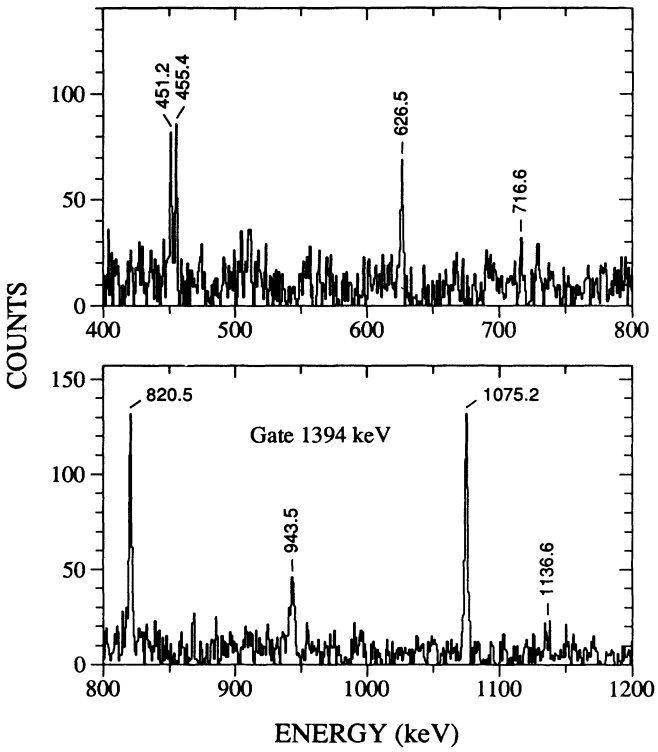

FIG. 2. Background-corrected coincidence spectrum gated on the 1394.4 keV transition in the (90°-90°) matrix.

B. Charged particle-γ coincidence measurement

To search for bands not feeding through the well-known $\frac{9}{2}^+$ level at 1000.2 keV a particle-γ coincidence measurement was performed. The same reaction as for the prompt γ-γ coincidence measurement was selected but on a Ni target of 14 mg/cm^2 thickness with natural isotopic abundance. The evaporated charged particles (protons and α particles) were detected with a ten-segment fast-slow phoswich detector array which surrounded the target in a close geometry. Each ΔE-E telescope detector consisted of a 50 μm thick plastic scintil-

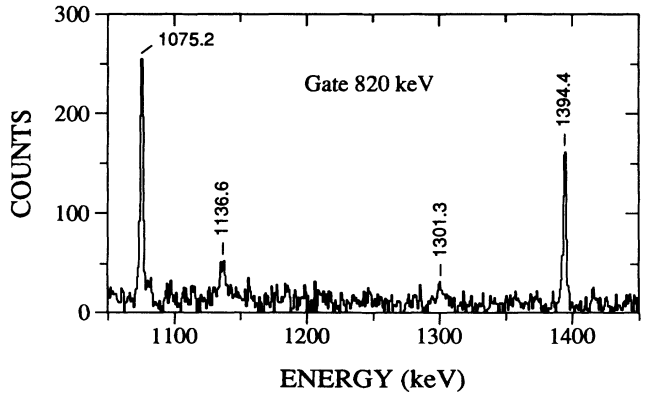

FIG. 3. Portion of a background-corrected γ-ray spectrum in coincidence with the 820 keV transition obtained from the (90°-4°) matrix.

TABLE I. Level energy, spins of initial and final states, γ-ray energy, intensity, DCO ratio, and multipolarity of transitions assigned to ^{71}As.

E_x (keV)	I_i^π	I_f^π	E_γ[a] (keV)	I_γ[b]	R_{DCO}	Multipolarity
147.5	$\frac{3}{2}^-$[c]	$\frac{5}{2}^-$	147.5(1)	22(4)[d]		$M1/E2$
924.7	$\frac{7}{2}^-$	$\frac{3}{2}^-$	777.4(3)	3(2)		$(E2)$
		$\frac{5}{2}^-$	924.6(2)	11(3)	0.36(8)	$M1/E2$
1000.2	$\frac{9}{2}^+$	$\frac{5}{2}^-$	1000.2(1)	100[e]	1.03(4)	$M2$
1129.3	$(\frac{5}{2}^+)$[c]	$\frac{3}{2}^-$	981.8(2)	6(1)		$(E1)$
1394.4	$\frac{9}{2}^-$	$\frac{7}{2}^-$	470.1(3)	≈ 1		$(M1/E2)$
		$\frac{5}{2}^-$	1394.4(2)	22(3)	1.09(9)	$E2$
1714.2	$\frac{13}{2}^+$	$\frac{9}{2}^+$	714.0(1)	70(5)	1.06(5)	$E2$
1728.6		$(\frac{5}{2}^+)$	599.3(2)	2(1)		
1798.3	$\frac{9}{2}^-$	$\frac{7}{2}^-$	873.7(2)	8(2)	0.44(11)	$M1/E2$
1816.7		$(\frac{5}{2}^+)$	687.4(2)	2(1)		
1904.3	$\frac{11}{2}^+$	$\frac{9}{2}^+$	904.1(2)	17(2)	0.28(5)	$M1/E2$
2110.8	$\frac{11}{2}^-$	$\frac{9}{2}^-$	312.6(3)	2(1)	0.36(12)	$(M1/E2)$
		$\frac{9}{2}^-$	716.6(3)	2(1)		$(M1/E2)$
		$\frac{9}{2}^+$	1110.4(3)	4(2)		$(E1)$
		$\frac{7}{2}^-$	1186.2(2)	7(2)	0.80(20)	$E2$
2416.1	$\frac{13}{2}^+$	$\frac{11}{2}^+$	511.9(5)	12(5)		$(M1)$
		$\frac{13}{2}^+$	701.9(2)	6(1)	0.74(9)	$M1/E2$
		$\frac{9}{2}^+$	1415.7(4)	3(1)	0.76(25)	$(E2)$
2469.6	$\frac{13}{2}^-$	$\frac{9}{2}^-$	671.5(3)	7(2)	1.04(17)	$E2$
		$\frac{9}{2}^-$	1075.2(1)	21(3)	1.06(8)	$E2$
2689.1	$\frac{17}{2}^+$	$\frac{13}{2}^+$	974.9(1)	41(4)	0.98(5)	$E2$
2748.3	$(\frac{13}{2}^+)$	$\frac{11}{2}^+$	844.0(3)	4(2)	0.34(9)	$M1/E2$
2793.1	$\frac{15}{2}^+$	$\frac{11}{2}^+$	889.0(3)	3(1)		$(E2)$
		$\frac{13}{2}^+$	1078.9(1)	20(2)	0.17(5)	$M1/E2$
2920.7	$\frac{15}{2}^-$	$\frac{13}{2}^-$	451.2(2)	5(2)	0.62(10)	$M1/E2$
		$\frac{11}{2}^-$	809.9(2)	6(2)	0.92(13)	$E2$
		$\frac{13}{2}^+$	1206.4(4)	8(2)	0.54(9)	$E1$
3237.3	$(\frac{17}{2}^+)$	$\frac{13}{2}^+$	821.2(3)	6(2)	1.10(11)	$(E2)$
3290.1	$\frac{17}{2}^-$	$\frac{13}{2}^-$	820.5(1)	22(3)	1.02(7)	$E2$
3601.8	$\frac{17}{2}^{(+)}$	$\frac{15}{2}^+$	808.7(3)	6(2)	0.27(8)	$(M1/E2)$
3789.2	$\frac{21}{2}^+$	$\frac{17}{2}^+$	1100.1(2)	19(2)	1.06(7)	$E2$
3916.6	$(\frac{19}{2}^-)$	$\frac{17}{2}^-$	626.5(2)	7(2)	0.51(10)	$M1/E2$
		$\frac{17}{2}^+$	679.5(3)	2(1)		$(E1)$
		$\frac{15}{2}^-$	995.9(3)	9(3)	1.28(22)	$(E2)$
		$\frac{17}{2}^+$	1227.2(5)	3(2)		$(E1)$
4233.6	$\frac{21}{2}^-$	$\frac{17}{2}^-$	943.5(2)	12(2)	1.05(9)	$E2$
4372.0		$\frac{19}{2}^-$	455.4(2)	5(1)	0.35(10)	$(M1/E2)$
4417.3	$\frac{19}{2}^{(-)}$	$\frac{17}{2}^+$	1728.2(5)	6(1)	0.62(8)	$(E1)$

TABLE I. *(Continued).*

E_x (keV)	I_i^π	I_f^π	E_γ[a] (keV)	I_γ[b]	R_{DCO}	Multipolarity
4463.0	$\frac{19}{2}(+)$	$\frac{17}{2}(+)$	861.5(3)	3(2)	0.66(17)	$(E1)$
		$\frac{17}{2}+$	1773.9(5)	6(1)	0.71(9)	$(E1)$
4763.7	$\frac{21}{2}(-)$	$\frac{19}{2}(-)$	300.5(1)	6(1)	1.29(9)	$M1/E2$
		$\frac{19}{2}(-)$	346.6(1)	4(1)	1.20(10)	$M1/E2$
		$\frac{21}{2}+$	974.7(3)	2(1)		$(E1)$
5022.0	$\frac{25}{2}+$	$\frac{21}{2}+$	1232.8(4)	10(2)	1.25(22)	$E2$
5073.2	$(\frac{23}{2}-)$	$(\frac{19}{2}-)$	1156.6(4)	≈ 2		$(E2)$
5370.2	$\frac{25}{2}-$	$\frac{21}{2}-$	1136.6(3)	7(2)	1.02(19)	$E2$
5822.8	$\frac{23}{2}(-)$	$\frac{21}{2}(-)$	1059.1(2)	10(3)	0.68(7)	$M1/E2$
5906.2		$\frac{21}{2}(-)$	1142.5(4)	4(2)		
6360.4	$(\frac{29}{2}+)$	$\frac{25}{2}+$	1338.4(4)	3(2)		$(E2)$
6671.5	$(\frac{29}{2}-)$	$\frac{25}{2}-$	1301.3(5)	2(1)		$(E2)$

[a]Uncertainties are given in parentheses.
[b]Intensities are given for 90°.
[c]Taken from Ref. [7].
[d]Includes contribution from β decay of ^{71}Se.
[e]Normalization.

lator with an aluminized front face for measuring the energy loss (ΔE) and a 9.5 mm thick plastic scintillator to measure the remaining energy (E) of the stopped particles. The γ rays were recorded with one Compton-suppressed Ge detector placed perpendicular to the beam axis. For each coincidence event ΔE, E, and timing information of the fired phoswich detectors was digitized and written to magnetic tape along with the Ge detector signal. In the off-line analysis, two-dimensional gates were set for the protons and for the α particles in each of the ten ΔE-E planes, and different γ-ray spectra were constructed according to the number of coincident protons and α's. A relevant example, a $1\alpha + 2p$ gated γ-ray spectrum is shown in Fig. 4 together with the total γ-ray projection of this coincidence experiment to illustrate the selectivity of the method. Due to misidentification of low-energy protons and α particles by about 15%, the particle gated γ-ray spectrum shown in Fig. 4 has been corrected for two other reactions with three particles in the outgoing channel, the (^{19}F,3p) and the (^{19}F,2α1p) reactions. The occurrence of the well-known γ rays at 714.0 and 1000.2 keV in Fig. 4 confirms the selectivity

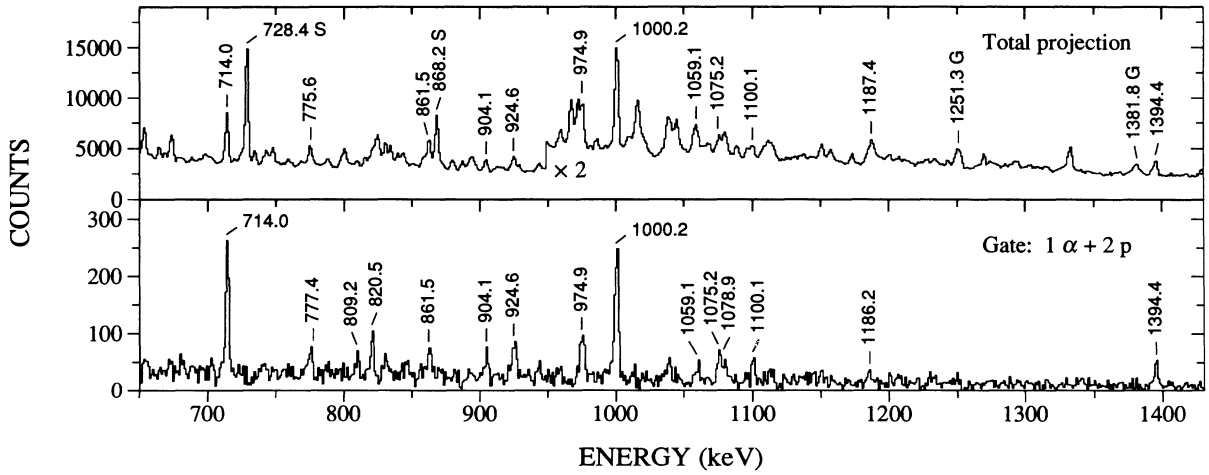

FIG. 4. Total γ-ray projection of the Ni + ^{19}F experiment (top) and background-corrected γ-ray spectrum in coincidence with one α particle and two protons (bottom). In the top spectrum a few strong lines are marked with their energy in keV, in particular with an additional label of G or S for those lines originating from the ^{58}Ni(^{19}F,2α1p)^{68}Ge or ^{58}Ni(^{19}F,3p)^{74}Se reactions, respectively. In the bottom spectrum the lines assigned to ^{71}As are marked.

for ^{71}As. The observation of a 1394.4 keV transition and some other new γ rays implies that previously unidentified states have been populated in ^{71}As.

III. ^{71}As LEVEL SCHEME

The level scheme for ^{71}As obtained in the present work is shown in Fig. 5. It contains several new γ rays and levels. The placement of the γ rays is primarily based on γ-γ coincidences, γ-ray intensities, and energy relations. There is a good agreement of our findings with previous work on the positive-parity yrast sequence but also some differences. Therefore, some details will be discussed next.

A. Negative-parity states

The well-known and firm $\frac{5}{2}^-$ assignment to the ^{71}As ground state is based on the measured proton orbital angular momentum transfer of $\ell_p = 3$ for the ground-state transition in the ^{70}Ge(^{3}He,d)^{71}As transfer reaction [5,6], on atomic beam magnetic resonance measurements [11], and on nuclear magnetic resonances of oriented ^{71}As [12] where an unequivocal spin of $\frac{5}{2}\hbar$ was found.

We have identified for the first time negative-parity states decaying to the ground state through a 1394.4 keV transition. This transition can be seen clearly in the γ-ray spectrum shown in Fig. 4 gated by one alpha and two protons. Its intensity implies that it feeds the ground state of ^{71}As directly. Thus, a new level at 1394.4 keV has been introduced. The γ rays in coincidence with the new transition, shown in Fig. 2, imply a number of new states above the 1394.4 keV level. A complete analysis of the prompt γ-γ coincidences leads to the new decay sequence shown on the right in the level scheme in Fig. 5. A number of these new transitions can also be seen in the 820 keV coincidence gate shown in Fig. 3 and in the particle-γ coincidence spectrum of Fig. 4. The observation of several decay branches to previously known positive-parity states, e.g., the 1206.4 keV γ-ray decay branch, provides further confirmation of the placement of the new decay sequence.

Previously, a 1395 keV γ ray [9] was found via the ^{69}Ga(α,$2n$)^{71}As reaction in coincidence with a 1075.9 keV line, the latter being the energy reported for the $(\frac{15}{2}^+) \rightarrow \frac{13}{2}^+$ transition. However, the 1395 keV transition was not placed in their decay scheme, presumably because it is not in coincidence with the 714.0 keV $\frac{13}{2}^+ \rightarrow \frac{9}{2}^+$ or the 1000.2 keV $\frac{9}{2}^+ \rightarrow \frac{5}{2}^-$ transitions. We distinguished the 1075 – 1079 keV doublet and could place both transitions in the ^{71}As level scheme, the 1078.9 keV in the unfavored sequence of positive parity and the 1075.2 keV in the new sequence of negative parity. In this way the observed coincidence pattern can be explained unambiguously.

In addition, a 1394.7 keV γ ray was observed [7] in the β decay of the $\frac{5}{2}^-$ ground state of ^{71}Se and in the (p,$2n\gamma$) reaction but it was not placed in their ^{71}As level scheme. The weak intensity of this γ ray in the decay study, similar to the observed intensity of the 1000.2 keV γ ray feeding the $\frac{9}{2}^+$ state in ^{71}As, points to a forbidden β-decay branch.

In order to determine DCO ratios for the transitions in the new decay sequence a stretched $E2$ multipolarity for the 1394.4 keV transition was assumed. It turned out that the γ rays at 1075.2, 820.5, 943.5, and 1136.6 keV show DCO ratios close to unity (see Table I). Therefore, they were interpreted as stretched $E2$ transitions. As a cross-check a DCO ratio of 1.09(9) was obtained for the 1394.4 keV transition from the 820.5 keV gate, thus con-

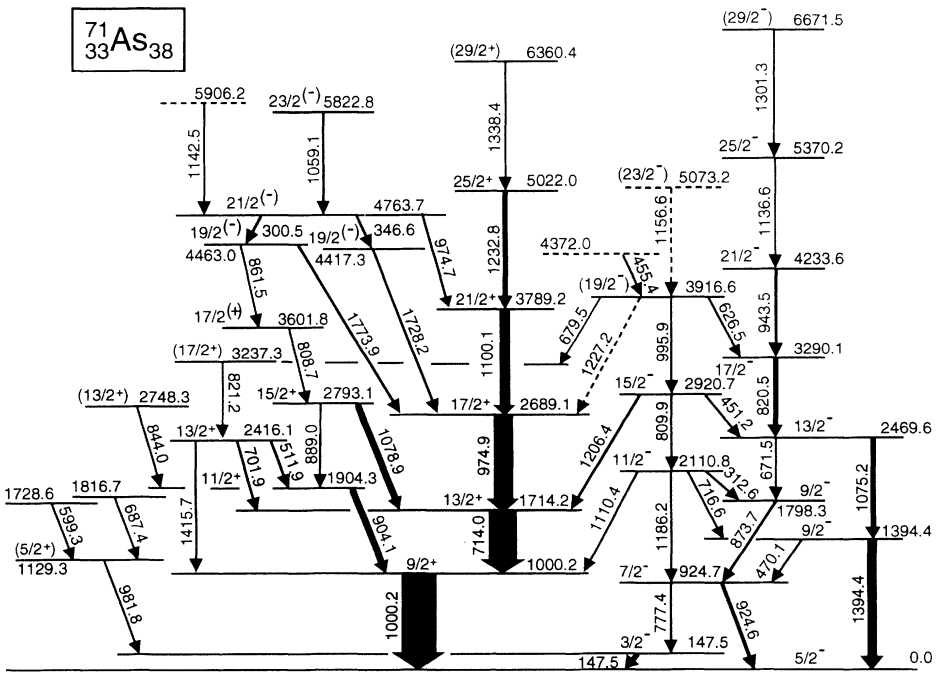

FIG. 5. Level scheme of ^{71}As deduced from the present work. The $\frac{3}{2}^-$, $\frac{9}{2}^+$, and $(\frac{5}{2}^+)$ assignments for the 147.5, 1000.2, and 1129.3 keV levels, respectively, have been taken from Refs. [7,9].

firming the initial $\Delta I = 2$ assumption for this line. The DCO ratios provide firm spin assignments up through the $\frac{25}{2}^-$ level. Systematic arguments suggest a spin $(\frac{29}{2}^-)$ for the highest member of this sequence.

Angular distribution coefficients and an excitation function were measured [10] for a 1395 keV transition in singles mode via the ^{61}Ni(^{12}C,pn)^{71}As reaction. The results of $a_2 = +0.203(16)$ and $a_4 = -0.03(9)$ are consistent with a $\Delta I = 2$ transition, and the excitation function fits a lower spin of the initial state better than the tentative placement on top of the positive-parity sequence as suggested in Ref. [10]. The lifetime of 6^{+5}_{-2} ps measured [10] for the 1395 keV line would imply a reasonable $B(E2)$ strength of 1.5(7) Weisskopf units (W.u.) but an unreasonable large $B(M2)$ strength of 83(40) W.u.

Hence, a firm $I^\pi = \frac{9}{2}^-$ assignment for the 1394.4 keV level has been made. The assignment of negative parity is consistent with the decay pattern of levels feeding primarily through the 1394.4 keV state. There is no detectable 394 keV branch to the $\frac{9}{2}^+$ 1000.2 keV level (< 2% of 1394.4 keV intensity).

The $\frac{7}{2}^-$ level at 924.7 keV has already been known from previous work [9,10]. We found several γ rays in prompt coincidence with the 924.6 keV transition; hence the unfavored decay sequence of negative parity could be identified. Spin assignments are based on the measured γ-ray DCO ratios obtained from the 809.9 keV gate, and on the DCO ratios of the linking transitions to the favored negative-parity sequence. The highest observed transition of 1156.6 keV is only tentatively placed due to limited statistics. The transition intensities in the unfavored sequence are weaker than those in the favored sequence. In summary, the observation of the $\frac{9}{2}^-$ and $\frac{11}{2}^-$ levels facilitates the identification of a signature-split band up to a spin of $(\frac{29}{2}^-)$.

A 414.3 keV transition in coincidence with the 924.6 keV γ ray as seen in Ref. [9] has not been found in our data set. Therefore, we cannot confirm the proposed $(\frac{9}{2}^-)$ level at 1339.3 keV.

A 455.4 keV γ ray has clearly been seen in all of our relevant coincidence gates and there is no doubt about its assignment to ^{71}As. However, a higher placement than indicated in the level scheme cannot be excluded since this γ ray forms a close-lying doublet with the strong $2^+ \rightarrow 0^+$ transition in ^{74}Kr [13] so that it is difficult to interpret weak coincidences.

B. $g_{9/2}$ band

The $I^\pi = \frac{9}{2}^+$ assignment for the isomeric level at 1000.2 keV is well established by the measured angular momentum transfer of $\ell_p = 4$ in the Ge(^{3}He,d) reaction [14] and by the measured angular distribution coefficients [9] for the intense 1000.2 keV transition to the $\frac{5}{2}^-$ ground state. Therefore, a firm $M2$ assignment was made in [9] for the 1000.2 keV γ ray. Moreover, the half-life of $T_{1/2} = 19.8(4)$ ns [15] implies a transition probability of $B(M2,\ 1000.2\ \text{keV}) = 0.091$ W.u. which is consistent with $M2$ decay strengths observed for $\frac{9}{2}^+ \rightarrow \frac{5}{2}^-$ transitions in some odd-neutron nuclei in this mass region [16] and tabulated values [17].

Levels on top of the $\frac{9}{2}^+$ isomer have been established by prompt coincidences of their depopulating γ rays with the lower-lying transitions in the sequence, including the 1000.2 keV γ ray. A relevant background-corrected spectrum is shown in Fig. 1. The lines in ^{71}As are marked, and the new transitions can be seen. Two new levels were added to extend the $\frac{9}{2}^+$ yrast band up to a $(\frac{29}{2}^+)$ state at 6360.4 keV excitation energy.

Our results confirm the yrast sequence known [9] up to spin $\frac{21}{2}\hbar$. Also a few known unfavored levels of positive parity could be confirmed with the exception that for the energy of the $\frac{15}{2}^+ \rightarrow \frac{13}{2}^+$ transition, which is given as 1075.9 keV in Ref. [9], a slightly larger value of 1078.9 keV has been observed. Based on our coincidence data the doublet structure of the peaks around this energy could be resolved and the close-lying 1075.2 keV transition has been placed in a negative-parity decay sequence of the ^{71}As level scheme (see Sec. III A).

The two previously identified states [9] with $\frac{11}{2}^+$ and $\frac{15}{2}^+$ have also been observed in our study but no $\frac{19}{2}^+$ state has been found. However, additional non-yrast states including a second $\frac{13}{2}^+$ state at 2416.1 keV have been identified. The relative intensities and $R_{\rm DCO}$ values for transitions in ^{71}As that decay through the 1000.2 keV level are included in Table I.

There are three other weak γ rays of 570.4, 924.1, and 1403.2 keV which show weak coincidences with the 714.0 and 1000.2 keV transitions. However, due to poor statistics they have not been placed in the level scheme.

C. Nonrotational structure

In addition to the positive-parity and negative-parity bands, we identified from our coincidence data a nonrotational high-lying structure in ^{71}As. This structure includes close-lying levels at 4417.3 keV and 4463.0 keV which decay to the $\frac{17}{2}^+$ level at 2689.1 keV through 1728.2 keV and 1773.9 keV transitions which do not show any Doppler shift. These levels are fed from a level at 4763.7 keV by low-energy transitions of 346.6 keV and 300.5 keV, respectively. The 300.5 keV transition had been placed in Refs. [9,10] as decaying directly into the $\frac{17}{2}^+$ level but we found a 1773.9 keV transition in between. The highest observed level in this structure, at 5822.8 keV, decays through a 1059.1 keV transition to the 4763.7 keV level.

The γ rays at 1728.2 and 1773.9 keV have $R_{\rm DCO}$ values of 0.62(8) and 0.71(9), respectively, which point to $\Delta I = 1$ transitions. Therefore, a spin of $\frac{19}{2}\hbar$ is assigned to each of the parent levels. For the low-energy γ rays at 300.5 and 346.6 keV the observed DCO ratios are larger then unity and point to mixed $\Delta I = 1$ transitions, and therefore a spin of $\frac{21}{2}\hbar$ is proposed for the level at 4763.7 keV. A comparison of the experimental DCO value of 1.29 for the 300.5 keV γ ray with theoretical predictions would imply a dipole-quadrupole mixing ratio of $\delta \approx -0.5$ which corresponds to an admixture of about 20% $E2$ multipolarity.

It should be mentioned that the 4463.0 keV level also decays via γ rays at 808.7 and 861.5 keV to the known

$\frac{15}{2}^+$ level at 2793.1 keV. The DCO ratios for these transitions support the $\frac{19}{2}$ assignment to the 4463.0 keV state. The DCO ratio of the 1059.1 keV γ ray suggests a spin $\frac{23}{2}\hbar$ for the 5822.8 keV. A transition of 1142.5 keV possibly feeds into the $\frac{21}{2}^{(-)}$ level but its placement is not well established due to missing coincidences in the high-energy γ-ray gates, maybe due to poor statistics. The parity of the levels involved in this high-lying structure is tentatively assigned as negative, as will be discussed in Sec. V D.

IV. LIFETIME MEASUREMENTS AND TRANSITION STRENGTHS

Lifetimes for high-spin states in ^{71}As were obtained from the analysis of Doppler-shifted lines shapes measured with the 4° Ge detector in coincidence with the 90° detectors, by means of the Doppler-shift attenuation method (DSAM). Background-subtracted coincidence spectra gated on transitions lying below the transition of interest were added together to improve the statistical accuracy for each set of data. The computer code FITI [18] was used to perform the analysis. This code simulates Doppler-shifted line shapes by taking into account the effects of the deceleration of the beam in the target before interaction, the distribution of recoil velocities, the detector resolution and geometry, direct feeding from known higher-lying states, and continuum side feeding. The electronic and nuclear stopping powers were taken from Ref. [19] and scaled by about 10% to the measured α stopping powers [20]. The angular straggling due to atomic collisions was treated in Blaugrund's approximation [21].

The lifetime for the highest level in a Doppler-shifted cascade was extracted first without any side-feeding time, and this result was used in FITI for calculations of lifetimes for lower levels. The side-feeding time was assumed in the present experiment to be 0.03 ps at 5 MeV excitation energy, and was assumed to increase by 0.03 ps per MeV of deexcitation, a choice that is typical for nuclei in the mass 70–80 region [22] produced in heavy-ion reactions.

The fit program performs a least-squares fit to the ob-

TABLE II. Level energy, spins of initial and final states, transition energy, lifetime, reduced $E2$ transition probability, and transition quadrupole moment of states in ^{71}As.

E_x (keV)	I_i^π	I_f^π	E_γ (keV)	τ^a (ps)	τ^b (ps)	$B(E2)$ (W.u.)[c]	$\lvert Q_t\rvert$ (eb)
924.7	$\frac{7}{2}^-$	$\frac{5}{2}^-$	924.6	3.0(25)[d]			
1394.4	$\frac{9}{2}^-$	$\frac{5}{2}^-$	1394.4	6^{+5}_{-2}[d]	> 2	1.5^{+7}_{-7}	
1714.2	$\frac{13}{2}^+$	$\frac{9}{2}^+$	714.0	5.7(6)[e]		44^{+5}_{-4}	1.90^{+11}_{-9}
				6.2(20)[d]			
1904.3	$\frac{11}{2}^+$	$\frac{9}{2}^+$	904.1	3(2)[d]	> 2		
2469.6	$\frac{13}{2}^-$	$\frac{9}{2}^-$	671.5		> 2	< 50	< 2.04
		$\frac{9}{2}^-$	1075.2			< 12	< 0.98
2689.1	$\frac{17}{2}^+$	$\frac{13}{2}^+$	974.9	0.9(3)[e]	0.69(22)	77^{+36}_{-19}	2.24^{+47}_{-29}
				2.3(15)[d]			
2793.1	$\frac{15}{2}^+$	$\frac{13}{2}^+$	1078.9		> 2		
3290.1	$\frac{17}{2}^-$	$\frac{13}{2}^-$	820.5		1.86(33)	68^{+15}_{-10}	2.10^{+22}_{-16}
3789.2	$\frac{21}{2}^+$	$\frac{17}{2}^+$	1100.1	≤ 1[d]	0.42(18)	69^{+52}_{-21}	2.02^{+65}_{-33}
4233.6	$\frac{21}{2}^-$	$\frac{17}{2}^-$	943.5		0.85(23)	74^{+27}_{-16}	2.08^{+36}_{-23}
4763.7	$\frac{21}{2}^{(-)}$	$\frac{19}{2}^{(-)}$	300.5	540(100)[d]			
				618(60)[e]			
5022.0	$\frac{25}{2}^+$	$\frac{21}{2}^+$	1232.8		0.30(10)	55^{+28}_{-14}	1.74^{+39}_{-23}
5370.2	$\frac{25}{2}^-$	$\frac{21}{2}^-$	1136.6		0.33(12)	75^{+43}_{-20}	2.04^{+52}_{-29}
5822.8	$\frac{23}{2}^{(-)}$	$\frac{21}{2}^{(-)}$	1059.1		> 2		
6671.5	$(\frac{29}{2}^-)$	$\frac{25}{2}^-$	1301.3		< 0.18	> 70	> 1.93

[a]Previous work.
[b]Present work.
[c]1 W.u. = 17.46 e^2 fm^4.
[d]Ref. [10].
[e]Ref. [8] (effective lifetime).

served line shape. The lifetime value with the smallest χ^2 is assigned as the lifetime of the level of interest. We were able to obtain the lifetimes of the 2689.1 keV ($\frac{17}{2}^+$), 3789.2 keV ($\frac{21}{2}^+$), and the 5022.0 keV ($\frac{25}{2}^+$) levels in the positive-parity yrast band and the 4233.6 keV ($\frac{21}{2}^-$) and 5370.2 keV ($\frac{25}{2}^-$) levels in the negative-parity band as well as an upper limit for the lifetime of the 6671.5 keV ($\frac{29}{2}^-$) level. Lifetime values for these levels are given in Table II, and examples of best fits are shown in Fig. 6. We were unable to obtain the lifetime of the 6360.4 keV ($\frac{29}{2}^+$) level due to limited statistics. The absence of Doppler shifts in the spectra of other transitions allows us to set a lower limit of $\tau > 2$ ps for their lifetimes. These include the 1394.4 keV (1394.4 keV γ ray), 1904.3 keV (904.1 keV γ ray), 2469.6 keV (1075.2 keV γ ray), 2793.1 keV (1078.9 keV γ ray), and 5822.8 keV (1059.1 keV γ ray) levels. Reduced transition probabilities $B(E2)$ for the affected $E2$ transitions were derived and are included in Table II. For comparison Table II also includes mean lifetimes reported in Refs. [8,10] for levels in ^{71}As deduced from Doppler-shift attenuation and recoil distance Doppler-shift measurements.

A quite long-lived component with $\tau = 618(60)$ ps was found [8] in the analysis of the 714 and 975 keV transitions but not assigned to a particular state. Later a lifetime of 540(100) ps was reported for a 300.1 keV transition [10]. All published data about this long lifetime can be understood if we assign it to the $\frac{21}{2}^-$ level at 4763.7 keV. It should be mentioned that the effect of the long feeding time of 540 ps from the 4763.7 keV level has been included in our DSA analysis of the 974.9 and 1100.1 keV transitions.

In addition to $E2$ transition probabilities we estimated $E1$ strengths for a few interband transitions that connect the signature-unfavored negative-parity band to the $\frac{9}{2}^+$ yrast band. These are the 1206.4 keV $\frac{15}{2}^- \rightarrow \frac{13}{2}^+$ and the tentative 1227.2 keV $\frac{19}{2}^- \rightarrow \frac{17}{2}^+$ transitions. We proceeded from the assumption that the $E2$ transitions in the unfavored negative-parity band have a collectivity similar to that of transitions in the favored band for which lifetimes were measured. From the branching ratios of the $E1$, $M1/E2$, and $E2$ transitions for a given level and taking into account the energy dependence of the matrix elements, we estimated $B(E1)$ values. For the 1206.4 keV line we obtained $B(E1) = 8 \times 10^{-5}\ e^2\ \mathrm{fm}^2$ and for the 1227.2 keV transition, $7 \times 10^{-5}\ e^2\ \mathrm{fm}^2$. These $B(E1)$ estimates are consistent with tabulated experimental $E1$ interband transition strengths in this region [17].

Transition quadrupole moments $|Q_t|$ were inferred from lifetime-derived $B(E2)$ strengths according to the rotational formula

$$Q_t^2 = \frac{16\pi}{5}\langle IK20|I-2K\rangle^{-2} B(E2, I \rightarrow I-2). \quad (2)$$

The $|Q_t|$ values obtained are listed in Table II and displayed in Fig. 7. For the intrinsic angular momentum a

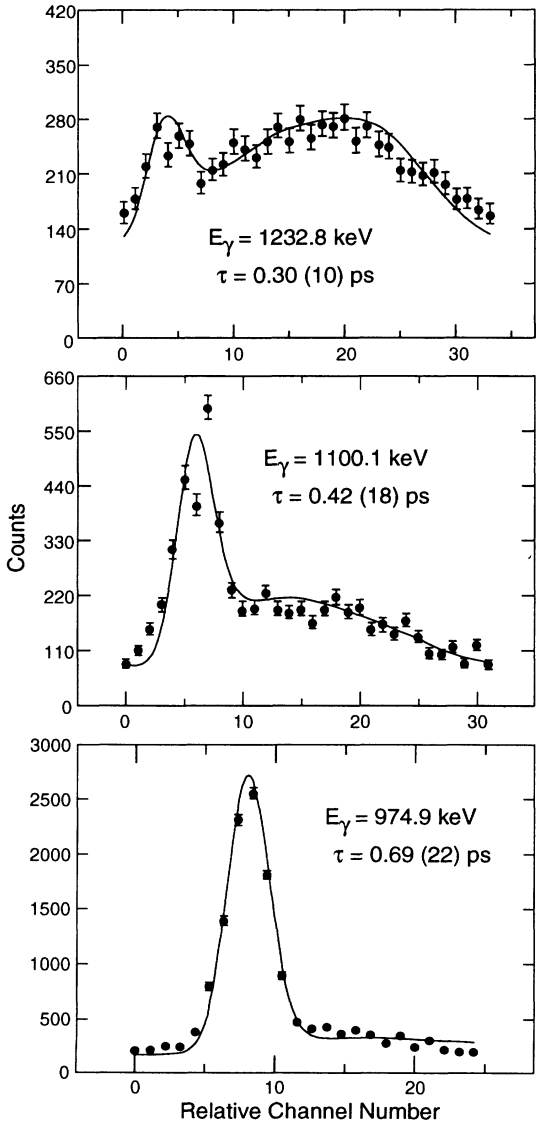

FIG. 6. Doppler-shifted line shapes observed in the forward direction. The smooth curves represent the best fits to the experimental data. Uncertainties in the data points are shown by vertical bars.

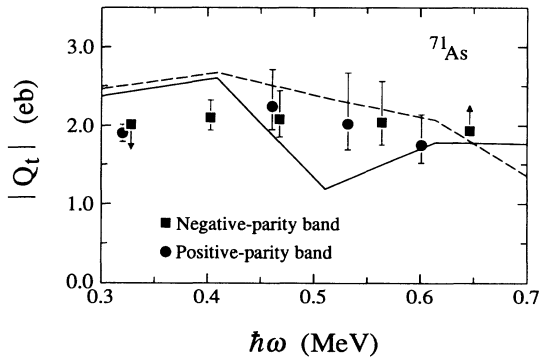

FIG. 7. Transition quadrupole moments deduced from the measured $E2$ transition probabilities in ^{71}As. The solid and dashed lines represent values obtained from the TRS minima given in Figs. 9 and 10 for positive- and negative-parity states, respectively.

K value of $\frac{5}{2}$ has been used for both the positive-parity and negative-parity bands.

V. DISCUSSION

A. Band structures and cranked-shell-model analysis

The $E2$ transitions in the positive-parity yrast band in ^{71}As show a quite high collectivity of $B(E2) \geq 40$ W.u. consistent with its interpretation as a rotational band. On the other hand, in the favored negative-parity sequence the reported lifetime for the 1394.4 keV transition leads to an $E2$ transition strength of 1.5 W.u. indicating single-particle structure. Rotational character only develops above about 2 MeV, as evidenced by the upper $B(E2)$ strength limits of 50 and 12 W.u. for the 671.5 and 1075.2 keV transitions, respectively, if the lower lifetime limit of 2 ps is used. Of the two $\frac{13}{2}^- \rightarrow \frac{9}{2}^-$ transitions from the 2469.6 keV level, the 1075.2 keV is more intense than the 671.5 keV. But the 671.5–1075.2 keV branching ratio leads to a higher $B(E2)$ limit for the 671.5 keV transition. If the negative-parity band is taken as commencing with the 671.5 keV transition, then the level energies show rotationlike spacings. These are similar to those in the negative-parity band in ^{71}Se [23], with, however, a difference of one unit in corresponding spins.

Due to the rotationlike properties we analyzed the observed sequences in ^{71}As in the framework of the cranked shell model. The kinematic moments of inertia $J^{(1)}$ and the dynamic moments of inertia $J^{(2)}$ were extracted for the $\frac{9}{2}^+$ yrast band and the negative-parity decay sequences built on the $\frac{9}{2}^-$ and $\frac{11}{2}^-$ states at 1798.3 and 2110.8 keV, respectively. The results are shown in Fig. 8. Both the moments of inertia $J^{(1)}$ and $J^{(2)}$ for the $\frac{9}{2}^+$ band increase slowly to $\hbar\omega = 0.67$ MeV, with no clear evidence of band crossings. The $J^{(1)}$ values obtained are about $(17\text{–}20)\hbar^2$/MeV for the $\frac{9}{2}^+$ band and are somewhat lower than the midshell values tabulated in Ref. [24].

For the negative-parity sequences somewhat larger, slowly increasing values of $J^{(1)}$ are obtained after the onset of collectivity. This onset occurs above $\hbar\omega = 0.32$ MeV if the 671.5 keV $\frac{13}{2}^- \rightarrow \frac{9}{2}^-$ transition is included in the collective band (as shown in Fig. 8), or only above $\hbar\omega = 0.39$ MeV if the 1075.2 keV $\frac{13}{2}^- \rightarrow \frac{9}{2}^-$ transition is considered. A weak peak in $J^{(2)}$ around 0.45 MeV may reflect a band crossing in the signature $\alpha = +\frac{1}{2}$ sequence.

B. Theoretical total Routhian surfaces

Total Routhian surfaces (TRS) were determined from Woods-Saxon Hartree-Fock-Bogolyubov (HFB) cranking calculations [25]. They were calculated as a function of the quadrupole deformation of the average nuclear matter distribution β_2^ν, triaxiality parameter γ, and rotational frequency $\hbar\omega$, and were minimized with respect to the hexadecapole deformation β_4 at each (β_2^ν, γ) point. A few samples of TRS plots for ^{71}As are shown in Fig. 9 for the positive-parity states with signature $\alpha = +\frac{1}{2}$ (denoted with $\pi = +$, $\alpha = +\frac{1}{2}$) and in Fig. 10 for negative-parity states (denoted with $\pi = -$, $\alpha = +\frac{1}{2}$), for $\hbar\omega = 0.3$, 0.5, and 0.7 MeV, which span the range of rotational frequencies observed in this study.

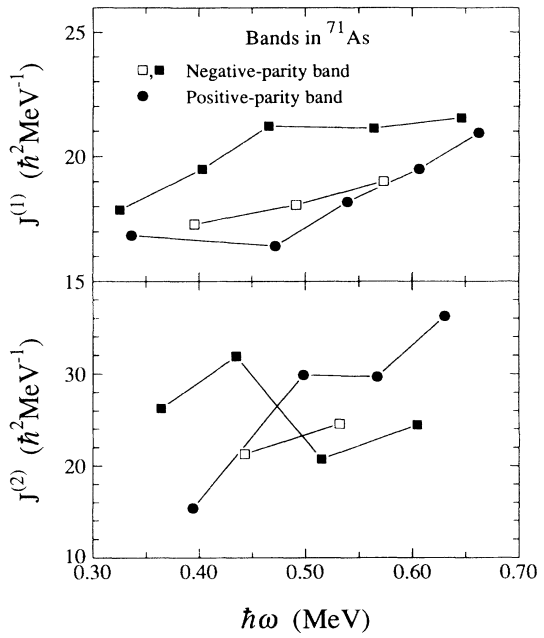

FIG. 8. Kinematic ($J^{(1)}$) and dynamic ($J^{(2)}$) moments of inertia for bands in ^{71}As. For the negative-parity sequences the $\frac{9}{2}^-$ and $\frac{11}{2}^-$ states at 1798.3 and 2110.8 keV, respectively, have been taken as lowest states. The sequences with signature $\alpha = +\frac{1}{2}$ and $-\frac{1}{2}$ are shown by solid and open symbols, respectively. The positive-parity band is built on the $\frac{9}{2}^+$ isomer. A value of $K = \frac{5}{2}$ has been used in the analysis of all bands.

The calculations predict ^{71}As to be very γ soft for positive-parity states at low rotational frequencies. At higher frequencies triaxial shapes with varying $\gamma > 0°$ values are obtained. Moderate to substantial deformations characterize the predicted shapes, with average quadrupole deformations β_2^ν of 0.25–0.34, and values near 0.3 predominant for higher $\hbar\omega$. Levels in the yrast $\frac{9}{2}^+$ band are characterized by fast $E2$ transitions, and so it is reasonable to associate the $\gamma > 0°$ ($\pi = +$, $\alpha = +\frac{1}{2}$) TRS minimum with this collective band.

The total Routhian calculations for negative-parity states with ($\pi = -$, $\alpha = +\frac{1}{2}$) as displayed in Fig. 10 show somewhat more complex results at low rotational frequencies. For $\hbar\omega$ below 0.4 MeV three shallow minima near 0° and ±60° are present, exhibiting the γ softness common near $A = 70$. From $\hbar\omega = 0.5$ upwards to 1 MeV the oblate minima are no longer present, as can be seen in Fig. 10. Below $\hbar\omega = 0.6$ MeV the band that is predicted to persist is nearly prolate but still γ soft. Above $\hbar\omega = 0.6$ MeV the negative-parity band is predicted to be triaxial with positive γ values like the positive-parity band discussed before.

It might be possible that one of the oblate minima calculated for rotational frequencies below 0.4 MeV is related to the new noncollective structure found at spins around $\frac{21}{2}^-$. This would lead to shape competition for

negative-parity states. However, we did not find any collective band built on the predicted collective oblate minimum.

Some earlier asymmetric rotor model calculations [4] for the positive-parity bands in ^{71}As and ^{73}As should be mentioned. These calculations used a fixed deformation of $\beta_2 \approx 0.25$ and a triaxiality of either $\gamma = 0°$ or $\gamma = 26.7°$ (corresponding roughly to $-26.7°$ in the TRS calculations). Both the large triaxiality and a variable moment of inertia improved the agreement of the calculated energies with the experimental energies in ^{73}As but the measured $B(E2)$ strength was significantly underpredicted. However, these results support large triaxiality in ^{71,73}As.

C. Triaxiality and transition quadrupole moments

It is worthwhile to compare the observed values of $|Q_t|$ to theoretical values obtained from (β_2^ν, γ) values corre-

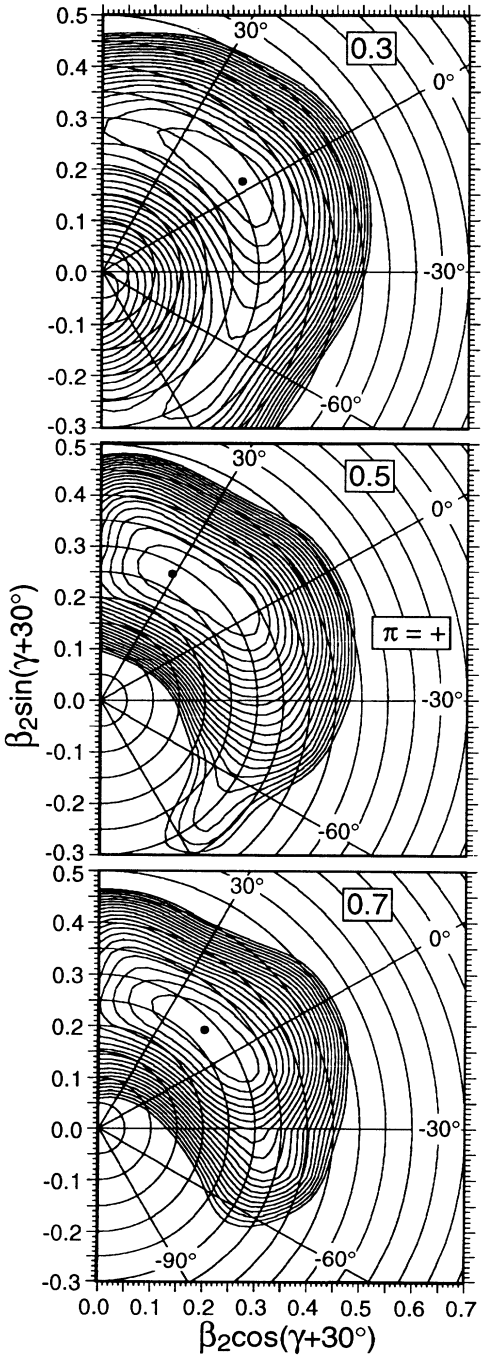

FIG. 9. Total Routhian surfaces in the (β_2^ν,γ) plane for the positive-parity configuration with signature $\alpha = +\frac{1}{2}$ in ^{71}As at rotational frequencies of $\hbar\omega = 0.3$, 0.5, and 0.7 MeV.

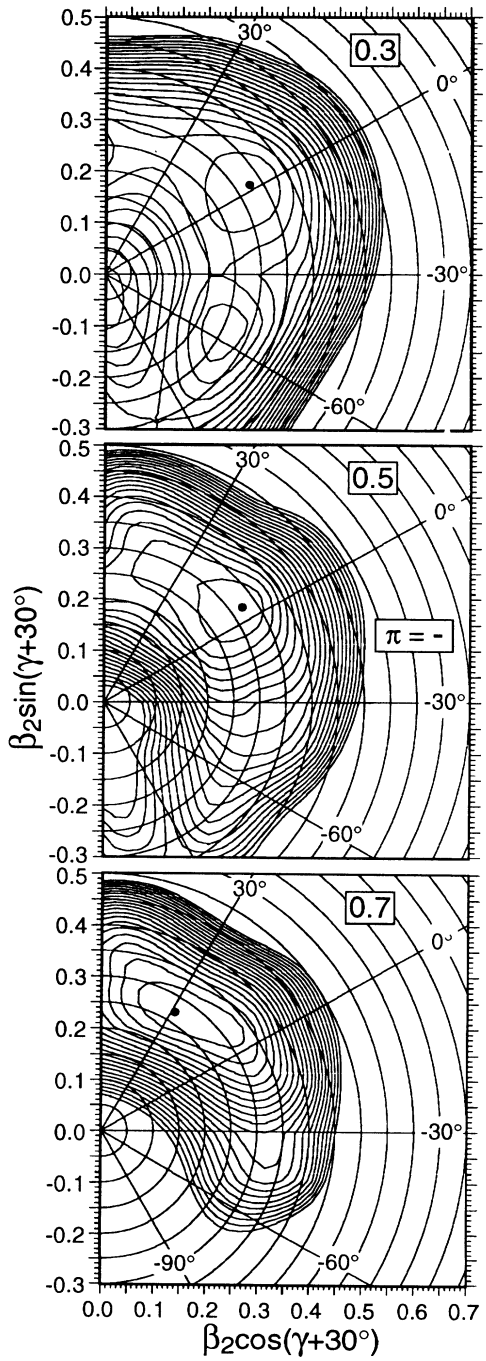

FIG. 10. Total Routhian surfaces for the negative-parity states with signature $\alpha = +\frac{1}{2}$ at the same frequencies as given in Fig. 9.

sponding to the TRS minima for the range of rotational frequencies for which we have experimental data.

The transition quadrupole moment $|Q_t|$ is related to the charge quadrupole deformation β_2^ρ in the case of axial symmetry according to the expression [26]

$$Q_t(\gamma = 0^\circ) = \left| \frac{6eZr_0^2A^{2/3}}{7\pi} \left\{ \left[\beta_2^\rho + 7\sqrt{\pi/80} \right]^2 - 49\frac{\pi}{80} \right\} \right|, \tag{3}$$

where $r_0 = 1.2$ fm was taken in our analysis. The charge quadrupole deformation β_2^ρ derived from $B(E2)$ transition strengths is related to the quadrupole deformation β_2^ν of the nuclear matter distribution derived from Woods-Saxon potential TRS calculations [26,27] by

$$\beta_2^\rho = 1.1\beta_2^\nu. \tag{4}$$

In order to take into account a possible triaxiality we used the high-spin limit for the γ dependence of $|Q_t|$ as given in Refs. [28,29]:

$$|Q_t| = (2/\sqrt{3})Q_t(\gamma = 0^\circ)|\cos(\gamma + 30^\circ)|, \tag{5}$$

where the transition quadrupole moment $|Q_t|$ is related to the moment at axial symmetry, $Q_t(\gamma = 0^\circ)$. Expression (5) indicates that moderate triaxiality corresponding to $\gamma > 0^\circ$ reduces $|Q_t|$ values substantially, while negative values for γ have relatively little effect until the collective oblate limit $\gamma = -60^\circ$ is approached.

The calculated $|Q_t|$ values, obtained from the TRS (β_2^ν, γ) values by means of Eqs. (3), (4), and (5), are shown in Fig. 7 as solid and dashed lines for positive- and negative-parity yrast states, respectively. It should be mentioned again that expression (5) assumes large angular momentum, which might be applicable for levels in ^{71}As with spins larger than $\frac{9}{2}\hbar$, e.g., states where a $g_{9/2}$ intruder quasiparticle is involved. The results in Ref. [28] for a triaxial rotor plus $h_{11/2}$ quasiparticle indicate that the high-spin limit is reached slowly for $\gamma > 0^\circ$, and that the high-spin case is a lower limit for $|Q_t|$.

The agreement between experimental and theoretical $|Q_t|$ values shown in Fig. 7 is rather better than might be expected, given the approximations involved. The experimental values are about constant with increasing angular frequency. The TRS results vary somewhat and the downward trend for the negative-parity band is caused by increasing triaxiality from about 0° up to 30° at higher rotational frequency.

D. Three-quasiparticle excitations

The previous discussion focused primarily on collective states observed in ^{71}As. However, a different approach seems to be appropriate for the structure of noncollective levels of negative parity observed at spins around $\frac{21}{2}\hbar$.

The observed levels can be interpreted as three-quasiparticle (qp) states originating from the coupling of a $g_{9/2}$ proton to the 5^- and 6^- states of the even-even ^{70}Ge core.

(i) In this way the spin, suggested parity, and excitation energy of the $\frac{21}{2}^{(-)}$ state can be well understood. The lowest 6^- state in the even-even Ge isotopes lies at an energy of 4321 keV in ^{66}Ge [30], at 3882 keV in ^{68}Ge [30], and at 3666 keV in ^{70}Ge [31,32]. By combining the 6^- energy of ^{70}Ge with the excitation energy of the proton $g_{9/2}$ excitation in ^{71}As we obtain an energy of 4666 keV, very close to the observed energy of the 4763.7 keV $\frac{21}{2}^{(-)}$ state in ^{71}As.

(ii) Similarly, a $\frac{19}{2}^{(-)}$ state in ^{71}As can be interpreted as coupling of a $g_{9/2}$ proton to the 5^- state in ^{70}Ge which is only 250 keV below the 6^- state. This would account for one of the two observed $\frac{19}{2}^{(-)}$ states in ^{71}As. In ^{66,68}Ge [30] two close-lying 5^- states are known but not in ^{70}Ge. However, from systematics also a second 5^- state is expected in ^{70}Ge.

(iii) The 6^- state in ^{70}Ge has a lifetime of $\tau = 51(4)$ ps [32] leading to $B(M1)$ and $B(E2)$ transition probabilities of 40 mW.u. and 0.8 W.u., respectively, for the mixed $6^- \rightarrow 5^-$ transition. In ^{71}As $B(M1)$ and $B(E2)$ transition strengths of 0.8 mW.u. and 3 W.u. (0.4 mW.u. and 1 W.u.) are obtained for the 300.5 keV (346.6 keV) transition, if the lifetime of 540 ps and a dipole-quadrupole mixing ratio of $\delta \approx -0.5$ (-0.4) are used. Furthermore, the 6^- level in ^{70}Ge is not involved in any $\Delta I = 2$ band. This points to a 2qp structure, however not necessarily to a two-quasiproton structure as discussed in Ref. [32]. A more complex nature is very likely, as pointed out for the negative-parity state in the lighter ^{66,68}Ge isotopes [30].

(iv) Based on this simple consideration a close-lying $\frac{23}{2}^-$ state would be expected for ^{71}As from the coupling of a $g_{9/2}$ proton to the 7^- state in ^{70}Ge which is only 288 keV above the 6^- level. We searched for such a close-lying level in ^{71}As but did not find it. Instead, a 5822.8 keV level with an assignment of $\frac{23}{2}^{(-)}$ has been identified which decays via an 1059.1 keV γ ray to the $\frac{21}{2}^{(-)}$ state. This may point to different structures of the 6^- and 7^- states in the ^{70}Ge core.

It should be mentioned that similar 3qp states of negative parity have been identified in ^{69}Ge [33] where a $g_{9/2}$ neutron is coupled to 5^-, 6^-, and 7^- states of the ^{68}Ge core. The above coupling is expected to occur also in other odd-mass nuclei of this mass region. Unfortunately the nuclei in the vicinity of ^{71}As such as ^{69,73}As or ^{71}Ge are not well investigated at high spins, preventing a more detailed systematic comparison.

VI. SUMMARY

In the present work the positive-parity yrast band in ^{71}As has been extended up to spin $(\frac{29}{2}^+)$. The $E2$ strengths deduced from lifetime measurements for transitions in this band show moderate to high collectivity. Total Routhian surface calculations suggest a quadrupole deformed but highly triaxial shape for this configuration in ^{71}As.

Many new states of negative parity up to spin $(\frac{29}{2}^-)$ have been identified in ^{71}As for the first time. The $E2$ transitions in the negative-parity band built on the second $\frac{9}{2}^-$ state also show a high collectivity. This band is

predicted to be triaxial and tends toward yrast at higher spins. On the other hand, a noncollective negative-parity structure has been found around spin $\frac{21}{2}\hbar$. These states can be understood as three-quasiparticle states resulting from the coupling of a $g_{9/2}$ proton to the 5^- and 6^- states of the ^{70}Ge core.

ACKNOWLEDGMENTS

The authors wish to thank W. Nazarewicz for making available the results of his TRS calculations. This work was supported in part by the Board of Regents of Louisiana and by the National Science Foundation.

[1] T.F. Lang, D.M. Moltz, J.E. Reiff, J.C. Batchelder, J. Cerny, J.D. Robertson, and C.W. Beausang, Phys. Rev. C **42**, R1175 (1990).
[2] A.R. Farhan and Shaheen Rab, Nucl. Data Sheets **60**, 735 (1990).
[3] A.R. Farhan, Shaheen Rab, and B. Singh, Nucl. Data Sheets **57**, 223 (1989).
[4] H. Toki and A. Faessler, Phys. Lett. **63B**, 121 (1976).
[5] L. Broman and B. Rosner, Nucl. Phys. **A114**, 237 (1968).
[6] R.R. Betts, S. Mordechai, D.J. Pullen, B. Rosner, and W. Scholz, Nucl. Phys. **A230**, 235 (1974).
[7] B.O. Ten Brink, P. Van Nes, C. Hoetmer, and H. Verheul, Nucl. Phys. **A338**, 24 (1980).
[8] B. Heits, H.-G. Friederichs, A. Gelberg, K.P. Lieb, A. Perego, R. Rascher, K.O. Zell, and P. von Brentano, Phys. Lett. **61B**, 33 (1976).
[9] B. Heits, H.-G. Friederichs, A. Rademacher, K.O. Zell, P. von Brentano, and C. Protop, Phys. Rev. C **15**, 1742 (1977).
[10] G.M. Gusinskii, V.S. Zvonov, I.Kh. Lemberg, and V.E. Mitroshin, Izv. Akad. Nauk SSSR, Ser. Fiz. **44**, 92 (1980).
[11] H.A. Helms, W. Hogervorst, G.J. Zaal, and J. Blok, Phys. Scr. **14**, 138 (1976).
[12] P. Herzog, N.J. Stone, and P.D. Johnston, Nucl. Phys. **A259**, 378 (1976).
[13] S.L. Tabor, P.D. Cottle, J.W. Holcomb, T.D. Johnson, P.C. Womble, S.G. Buccino, and F.E. Durham, Phys. Rev. C **41**, 2658 (1990).
[14] R.R. Betts, D.J. Pullen, W. Scholz, and B. Rosner, Phys. Rev. Lett. **26**, 1576 (1971).
[15] M. Becker, H. Bertschat, U. Leithauser, W. Leitz, H.-E. Mahnke, E. Recknagel, W. Semmler, R. Sielemann, B. Spellmeyer, W. Wasserthal, and T. Wichert, HMI Report No. 112, 1971, p. 58; H. Bertschat, H. Haas, W. Leitz, U. Leithäuser, K. H. Maier, H.-E. Mahnke, E. Recknagel, W. Semmler, R. Sielemann, B. Spellmeyer, and Th. Wichert, J. Phys. Soc. Jpn. **34**, 217 (1973); K.R. Alvar, Nucl. Data Sheets **10**, 205 (1973).
[16] J.W. Arrison, D.P. Balamuth, T. Chapuran, D.G. Popescu, J. Görres, and U.J. Hüttmeier, Phys. Rev. C **40**, 2010 (1989).
[17] P.M. Endt, At. Data Nucl. Data Tables **23**, 547 (1979).
[18] E.F. Moore, P.D. Cottle, C.J. Gross, D.M. Headly, U.J. Hüttmeier, S.L. Tabor, and W. Nazarewicz, Phys. Rev. C **38**, 696 (1988).
[19] L.C. Northcliffe and R.F. Schilling, Nucl. Data Tables A **7**, 233 (1970).
[20] J.F. Ziegler and W.K. Chu, At. Data Nucl. Data Tables **13**, 463 (1974).
[21] A.E. Blaugrund, Nucl. Phys. **88**, 501 (1966).
[22] S.G. Buccino, F.E. Durham, J.W. Holcomb, T.D. Johnson, P.D. Cottle, and S.L. Tabor, Phys. Rev. C **41**, 2056 (1990).
[23] A.V. Ramayya, Nucl. Instrum. Methods B **40/41**, 432 (1989).
[24] S.L. Tabor, Phys. Rev. C **45**, 242 (1992).
[25] W. Nazarewicz, J. Dudek, R. Bengtsson, T. Bengtsson, and I. Ragnarsson, Nucl. Phys. **A435**, 397 (1985).
[26] W. Nazarewicz, M.A. Riley, and J.D. Garrett, Nucl. Phys. **A512**, 61 (1990).
[27] J. Dudek, W. Nazarewicz, and P. Olanders, Nucl. Phys. **A420**, 285 (1984).
[28] I. Hamamoto and B.R. Mottelson, Phys. Lett. **132B**, 7 (1983).
[29] P. Ring, A. Hayashi, K. Hara, H. Emling, and E. Grosse, Phys. Lett. **110B**, 423 (1982).
[30] U. Hermkens, F. Becker, J. Eberth, S. Freund, T. Mylaeus, S. Skoda, W. Teichert, and A. v.d. Werth, Z. Phys. A **343**, 371 (1992).
[31] R.L. Robinson, H.J. Kim, R.O. Sayer, J.C. Wells, R.M. Ronningen, and J.H. Hamilton, Phys. Rev. C **16**, 2268 (1977).
[32] L. Cleemann, J. Eberth, W. Neumann, and V. Zobel, Nucl. Phys. **A386**, 367 (1982).
[33] T. Paradellis, G.J. Costa, R. Seltz, C. Lebrun, D. Ardouin, F. Guilbault, M. Vergnes, and G. Berrier, Nucl. Phys. **A330**, 216 (1979).